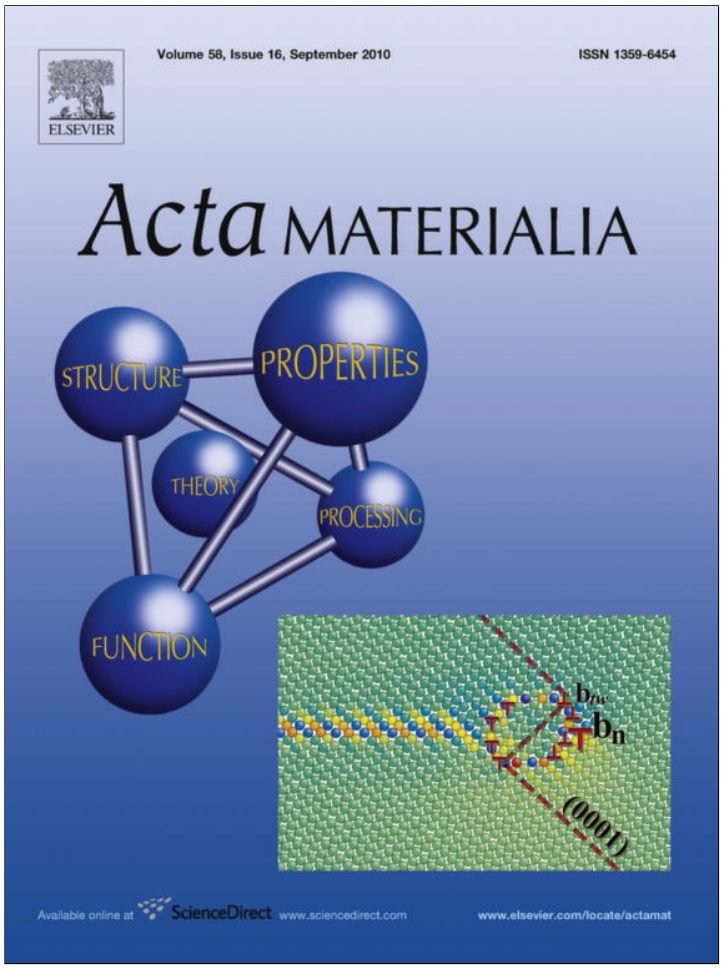

Available online at www.sciencedirect.com
ScienceDirect
Acta Materialia 58 (2010) 5286–5294
Acta MATERIALIA
www.elsevier.com/locate/actamat

Ductile vs. brittle behavior of pre-cracked nanocrystalline and ultrafine-grained materials

I.A. Ovid'ko *, A.G. Sheinerman

Institute of Problems of Mechanical Engineering, Russian Academy of Sciences, Bolshoj 61, Vasilievskii Ostrov, St. Petersburg 199178, Russia

Received 26 February 2010; received in revised form 28 May 2010; accepted 30 May 2010
Available online 25 June 2010

Abstract

Aspects of the ductile vs. brittle response of nanocrystalline and ultrafine-grained (UFG) materials are theoretically examined. The focus of this study is on the combined effects of grain boundaries (GBs) and blunting of cracks on the fracture toughness of nanocrystalline and UFG materials in a typical situation where crack blunting and growth processes are controlled by dislocation emission from crack tips. Within our description, lattice dislocations emitted from cracks are stopped at GBs, resulting in blunting of cracks. Both crack blunting and the stress fields of the arrested dislocations hamper further dislocation emission from cracks in nanocrystalline and UFG materials. As a result, crack blunting is suppressed, while crack growth is enhanced. The combined effects of GBs and blunting of cracks on the dislocation emission, further crack blunting and growth processes depend on grain size and material parameters. The dependence of the maximum number of dislocations, emitted by a crack, and the critical stress intensity factor on grain size (ranging from 10 to 300 nm) in Al and α-Fe is calculated. It is demonstrated that a decrease in grain size from 300 to 10 nm in Al and α-Fe decreases their critical stress intensity factors by a factor of 2–3 and thereby dramatically reduces the toughness/ductility of these materials.

Keywords: Fracture; Plastic deformation; Nanocrystalline materials

1. Introduction

In general, nanocrystalline materials show superior strength but at the expense of both low tensile ductility and low fracture toughness, limiting the structural applications of these materials (e.g. [1–10]). In particular, the tendency of nanocrystalline materials to have low fracture toughness is illustrated clearly by the experimental fact that some nanocrystalline metals with the face-centered-cubic (fcc) lattice exhibit a ductile-to-brittle transition with decreasing grain size [11–13]. In contrast, good ductility is always inherent in coarse-grained fcc metals where emission of lattice dislocations from cracks causes effective blunting of cracks and thus suppresses their growth (e.g. [14–16]). The difference in fracture behavior between nanocrystalline and coarse-grained fcc metals can be attributed to the difference in the role of the lattice dislocation slip in deformation processes in these materials. Lattice dislocation slip serves as the dominant deformation mode in both coarse-grained polycrystalline metals over wide temperature ranges and microcrystalline ceramics at elevated temperatures. Grain boundaries (GBs) thus serve as obstacles to dislocation slip and thereby control grain size effects on plastic flow and fracture processes in polycrystalline materials [17,18]. When the grain size of a material decreases down to the nanometer scale, lattice dislocation slip is hampered or even completely suppressed [1–10], because GBs (which exist in very large numbers in nanocrystalline materials) arrest gliding lattice dislocations. In addition, dislocation generation is suppressed in nanoscale grains due to the size effect preventing the activity of lattice dislocation sources, such as Frank–Read sources (e.g. [19]). However, the latter factor does not operate near cracks (because lattice dislocations can be generated at crack-free surfaces), and lattice dislocation slip can come into play. For instance, Kumar et al. [20]

* Corresponding author.
E-mail address: ovidko@nano.ipme.ru (I.A. Ovid'ko).

1359-6454/$36.00 © 2010 Acta Materialia Inc. Published by Elsevier Ltd. All rights reserved.
doi:10.1016/j.actamat.2010.05.058

reported the "in situ" observation (by high-resolution electron microscopy) of lattice dislocation emission from a crack tip during deformation of nanocrystalline Ni. In this context, there is great interest in identifying the specific features of lattice dislocation slip near crack tips and its effects on crack growth in nanocrystalline materials.

Previous works [21–23] considered the effect of GBs on dislocation emission from the tip of a semi-infinite crack [21,22] or dislocation sources near the crack tip [23] in polycrystalline materials. They have demonstrated that fracture toughness decreases with a decrease in grain size if gliding dislocations are arrested at GBs. The influence of the blunting radius, characterizing crack tip curvature, on fracture toughness has been investigated in Refs. [23–27]. It appears that fracture toughness decreases with a decrease in the crack tip radius, at least until the crack tip radius becomes smaller than some critical value at which fracture toughness reaches a constant limiting value. In a short paper [28], we briefly discussed the role of GBs in stopping lattice dislocations emitted from a crack tip and thus limiting crack blunting in nanocrystalline materials. At the same time, besides GBs, crack blunting itself strongly influences dislocation emission from a crack tip [2]. That is, in general, both GBs and crack blunting cause the combined effects on dislocation emission from crack tips in nanocrystalline materials. In its turn, dislocation emission from crack tips strongly influences crack blunting and growth processes. The main aim of this paper is to describe theoretically the combined effects of GBs and crack blunting on the toughness of nanocrystalline materials in a typical situation where crack blunting and growth processes are controlled by dislocation emission from crack tips.

In this paper we will also extend the suggested theoretical approach [28] to a description of the combined effects of GBs and crack blunting on the toughness of ultrafine-grained (UFG) metallic materials. Such materials are commonly produced by severe plastic deformation methods and have very high strength, several times larger than that of their coarse-grained counterparts [29–31]. Furthermore, there are examples of UFG materials characterized by both high strength and good ductility or even superplasticity [31–34]. The fundamental nature of this combination of high strength and good ductility of UFG materials has been the subject of intensive discussions [31–34]. We think that the suppression of crack growth due to dislocation emission from cracks is one of the key factors enhancing the mechanical properties of UFG metallic materials. In this paper, we will consider the sensitivity of fracture toughness to the grain size in UFG materials, while also taking into account the combined effects of GBs and crack blunting on the dislocation emission from cracks.

2. Lattice dislocation emission from crack tips in nanocrystalline and ultrafine-grained materials: model

Let us consider a nanocrystalline solid under a remote one-axis tensile loading (Fig. 1). The solid is supposed to

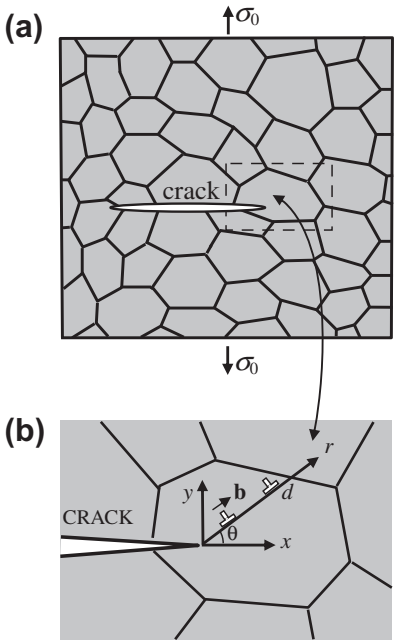

Fig. 1. Crack in a deformed nanocrystalline or UFG-grained solid. (a) General view. (b) Magnified inset highlighting generation of edge dislocations near the tip of a long crack.

be elastically isotropic and have the shear modulus G and Poisson ratio ν. Let a long flat crack grow in the solid, as is schematically shown in Fig. 1. If the stress intensity near the crack tip is large enough, the crack induces plastic shear through the emission of a lattice dislocation from the crack tip (Fig. 1). Since GBs serve as obstacles for lattice dislocation slip [1–10], we assume that the emitted dislocation is retarded at the neighboring GB. In general, the emission of the first dislocation is followed by the emission of further dislocations along the same slip plane. These new dislocations slip until they reach their equilibrium positions determined by the balance of the force exerted by the applied shear stress (which promotes dislocation slip) and the force exerted by the previously emitted dislocations (which hinders dislocation slip).

If the grain size of the solid is sufficiently large, the emitted dislocations move far enough from the crack tip and do not significantly hinder the motion of new dislocations until the number of the emitted dislocations becomes large enough. In this case, the dislocation emission along one slip plane can induce significant blunting of the crack tip. Following Refs. [14,16,35], significant crack blunting arrests crack growth and makes the solid ductile. At the same time, in nanomaterials, the emission of even one dislocation and its arrest at the nearest GB hinder the emission of subsequent dislocations along the same plane due to dislocation repulsion. In doing so, dislocation emission does not induce significant crack blunting. As a corollary, the nanocrystalline solid tends to show a brittle behavior.

Note that the above scenario is realized in the situation where slip of lattice (perfect or partial) dislocations dominates in nanocrystalline materials. In particular, it is the

case for room temperature deformation of nanocrystalline and UFG metals with a grain size d larger than the critical size $d_c \approx 20$ nm [5,7–9]. In these materials, emission of lattice dislocations from the crack tips is expected to be the dominant micromechanism for crack blunting at room temperature. Our view is supported by the experimental "in situ" observation [20] of lattice dislocation emission from a crack tip in nanocrystalline Ni with mean grain size $d = 23$ nm. In contrast, GB sliding plays an important or even dominant role in plastic flow in nanocrystalline metals with the finest grains ($d < 20$ nm) at room temperature, and in nanocrystalline metals and ceramics with widely ranging grain sizes at elevated temperatures [5,7–9]. In these materials, both lattice slip and GB sliding are expected to contribute to the blunting of cracks. This view is supported by computer simulations [36] showing that lattice dislocation emission and GB deformation processes contribute approximately 60% and 40%, respectively, to the blunting of a crack in nanocrystalline α-Fe with grain size $d = 9$ nm. In this paper, for definiteness, we consider the emission of only lattice dislocations from cracks. In doing so, our model effectively describes crack blunting in nanocrystalline and UFG metals with grain sizes $d > 20$ nm at room temperature and approximately describes crack blunting in other nanocrystalline materials.

Following Ref. [28], a decrease in the grain size of a nanocrystalline or UFG solid reduces the number of dislocations that can be emitted from the crack tip and thus hinders considerable crack blunting and makes the solid more brittle. At the same time, crack blunting itself influences dislocation emission. In particular, according to Beltz et al. [35], an increase in the crack tip curvature radius (resulting from crack blunting) hinders both crack growth and subsequent dislocation emission, and can in some cases lead to the transition from the ductile to the brittle mode of failure. In the following, we will study the combined effect of GBs and crack blunting on the fracture toughness of a nanocrystalline metallic or UFG solid. To do so, in the following sections, we consider a blunt crack and compare the conditions for its growth and those for dislocation emission from the crack tip.

3. Conditions for growth of blunt cracks in nanocrystalline and ultrafine-grained materials

Let us consider a crack in a nanocrystalline or UFG specimen. Following the approach in Refs. [35,37], we model the crack as an elongated ellipse with a curvature radius ρ at the crack tip, which is much smaller than the crack half-length a (Fig. 2). (The crack tip curvature radius ρ is related to the ellipse semi-axes a and p as $\rho = p^2/a$.) We also introduce a Cartesian coordinate system (x, y) with the origin at the ellipse center and a polar coordinate system (r, θ) with the origin at the right edge of the ellipse. In the Cartesian coordinate system, the stress σ_{yy} created by the external tensile load at the tip of the elliptical crack has the following relationship with the crack tip curvature radius ρ [35,38]:

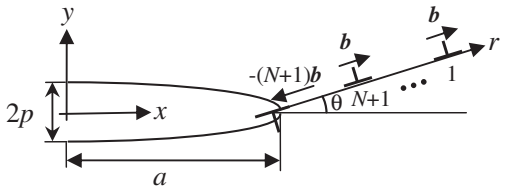

Fig. 2. Dislocations near a blunt crack described by an ellipse.

$$\sigma_{yy}(x = a, y = 0) = \frac{2K_I}{\sqrt{\pi\rho}}, \tag{1}$$

where K_I is the generalized stress intensity factor [37] assuming that the ellipse is replaced by a sharp crack. (It should be noted that the crack tip radius ρ in Eq. (1) and in our subsequent analysis is used in the same manner as done for the plastic zone size in other model fracture mechanics descriptions—e.g. [39,40].)

Following Ref. [35], we also suppose that the growth of the blunt crack occurs if the tensile stress σ_{yy} at the crack tip reaches some critical value σ_p ($\sigma_{yy} = \sigma_p$). Within the macroscopic description (which does not consider details of the process at the crack tip), the crack grows if $K_I = K_{IC}$. Combining this with the relation $\sigma_{yy}(x = a, y = 0) = \sigma_p$ and formula (1), we obtain:

$$K_{IC} = \frac{\sigma_p\sqrt{\pi\rho}}{2}. \tag{2}$$

Formula (2) is valid when ρ is larger than some critical radius ρ_c at which the crack tip can be considered as curved. In the case of $\rho = 0$ (sharp crack), we use the formula [41] $K_{IC} = K_{IC}^{\mathrm{br}} = \sqrt{4G\gamma/(1-\nu)}$, where γ is the specific surface energy.

Following Ref. [35], we define ρ_c by the equality:

$$K_{IC}^{\mathrm{br}} = \frac{\sigma_p\sqrt{\pi\rho_c}}{2}, \tag{3}$$

which gives $\rho_c = 16G\gamma/[\pi(1-\nu)\sigma_p^2]$, and put:

$$K_{IC} = \begin{cases} \sqrt{4G\gamma/(1-\nu)}, & \rho < \rho_c, \\ \frac{\sigma_p\sqrt{\pi\rho}}{2}, & \rho > \rho_c. \end{cases} \tag{4}$$

Let us use formula (4) in order to estimate K_{IC} for Al and α-Fe. In the case of Al, we use the following parameter values: $\sigma_p = 9.06$ GPa, $\gamma = 0.56$ J m^{-2} ([35] and references therein), $G = 27$ GPa and $\nu = 0.34$. For α-Fe, we have: $\sigma_p = 31.7$ GPa, $\gamma = 1.42$ J m^{-2} ([35] and references therein), $G = 82$ GPa and $\nu = 0.29$. With these characteristic values of parameters, we calculated the dependences $K_{IC}(\rho)$ for Al and α-Fe; these are shown in Fig. 3. It follows from Fig. 3 that $\rho_c \approx 1.4$ nm for Al, and $\rho_c \approx 0.8$ nm for α-Fe.

4. Dislocation emission from blunt cracks in nanocrystalline and ultrafine-grained materials

Now let us consider dislocation emission from the tip of a blunt crack. Let the first dislocation be emitted from the crack tip and stop at the neighboring GB. Then the follow-

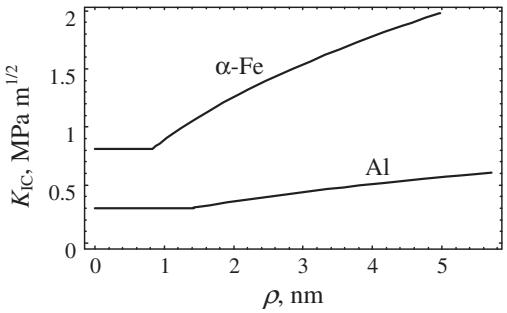

Fig. 3. Dependence of the critical stress intensity factor K_{IC} on the crack tip curvature radius ρ for Al and α-Fe.

ing dislocations are emitted and move along the same slip plane until they reach their equilibrium positions. Our goal here is to calculate the maximum number of dislocations that can be emitted along the same slip plane as a function of the grain size d and crack tip curvature radius ρ. To do so, we consider the situation where N dislocations have already been emitted from the crack tip and are located at their equilibrium positions and calculate the total force that would act on the $(N+1)$th emitted dislocation. We also take into account that every dislocation emitted from an internal crack of finite extent produces an opposite dislocation inside the crack. That is, if one constructs a Burgers contour around the internal crack of finite length, one obtains a non-zero Burgers vector characterizing the crack. As a consequence, after the emission of $(N+1)$ dislocations with the Burgers vector b from the crack tip, the dislocation with the Burgers vector $-(N+1)\mathbf{b}$ forms inside the crack (see Fig. 2). The stress field of this dislocation does not depend on its position inside the crack, as was noted by Eshelby [42]. In other words, the internal crack is characterized by the dislocation Burgers vector $-(N+1)\mathbf{b}$ and may be considered as a superdislocation with a hollow elliptical core coinciding with the crack profile. (This situation resembles that with dislocated micropipes treated as superdislocations having hollow cylindrical cores with large radii in semiconductors [43–49].)

The projection F of the total force, acting on the $(N+1)$th emitted dislocation, onto the r-axis can be written as:

$$F(r,\theta) = F^{\mathrm{emit}}(r,\theta) + F^{im}(r,\theta) + \sum_{k=1}^{N} F^{d-d}(r_k, r, \theta) - (N+1)F^{d-d}(0, r, \theta), \tag{5}$$

where $F^{\mathrm{emit}}(r,\theta)$ is the projection of the force exerted by the stress field created by the applied load in the vicinity of the crack tip onto the r-axis, $F^{im}(r,\theta)$ is the projection of the image force, acting on the dislocation, onto the r-axis, $F^{d-d}(r_k, r, \theta)$ is the projection of the force that the kth dislocation exerts on the $(N+1)$th dislocation onto the r-axis, and $-(N+1)F^{d-d}(0, r, \theta)$ is the projection of the force that the dislocation inside the elliptical crack exerts on the $(N+1)$th emitted dislocation. For brevity, in the following, the quantities F, F^{emit}, F^{im} and F^{d-d} will be referred to as forces but we will imply that these denote the projections of the corresponding forces onto the r-axis.

The force $F^{\mathrm{emit}}(r,\theta)$ follows as $F^{\mathrm{emit}} = b\sigma_{r\theta}$, where b is the magnitude of the dislocation Burgers vector and $\sigma_{r\theta}$ is the component of the stress field created by the applied tensile load σ_0 near the tip of the elliptical crack. The stress $\sigma_{r\theta}$ can be found [47] from:

$$\sigma_{r\theta} = \mathrm{Im}[(\bar{z}\varphi''(z) + \psi'(z))e^{2i\theta}], \tag{6}$$

where ϕ and ψ are the complex potential given by (e.g. [48]):

$$\varphi = \frac{\sigma_0 R}{4}\left(\xi - (2+m)\frac{1}{\xi}\right),$$
$$\psi = \frac{\sigma_0 R}{2}\left(\xi - \frac{1}{\xi} - \frac{(1+m)(1+m\xi^2)}{\xi(\xi^2 - m)}\right), \tag{7}$$

$z = x + iy = a + re^{i\theta}$, $i = \sqrt{-1}$, the overbar denotes the complex conjugate, $R = \sqrt{a}(\sqrt{a} + \sqrt{\rho})/2$, $m = (\sqrt{a} - \sqrt{\rho})/(\sqrt{a} + \sqrt{\rho})$, and ξ is one of the two roots of the equation $z = R(\xi + m/\xi)$, such that $|\xi| \geqslant 1$.

The image force $F^{im}(r,\theta)$ acting on the dislocation is calculated [49] as:

$$F^{im}(r,\theta) = b\lim_{r_0 \to r}\left[\sigma^{im}_{r\theta}(r_0, r, \theta)\right], \tag{8}$$

where $\sigma^{d}_{r\theta}(r_0, r, \theta)$ is the image stress that a dislocation located at the point (r,θ) creates in the point (r_0,θ) located in the vicinity of the elliptical crack tip. The stress $\sigma^{im}_{r\theta}(r_0, r, \theta)$ is calculated [48] using the complex potentials ϕ_{im} and ψ_{im} as:

$$\sigma^{im}_{r\theta} = \mathrm{Im}[(\bar{z}\varphi''_{im}(z) + \psi'_{im}(z))e^{2i\theta}], \tag{9}$$

where

$$\varphi_{im}(z) = 2A\ln\xi - A\ln\left(\xi - \frac{m}{\bar{\xi}_d}\right) - A\ln\left(\xi - \frac{1}{\bar{\xi}_d}\right) + \bar{A}\frac{\xi_d(1 + m\bar{\xi}_d^2) - \bar{\xi}_d(\xi_d^2 + m)}{\xi_d\bar{\xi}_d(\bar{\xi}_d^2 - m)(\xi - 1/\bar{\xi}_d)}, \tag{10}$$

$$\psi_{im}(z) = 2\bar{A}\ln\xi - \bar{A}\ln\left(\xi - \frac{m}{\xi_d}\right) - \bar{A}\ln\left(\xi - \frac{1}{\bar{\xi}_d}\right) + A\frac{\bar{\xi}_d(\xi_d^2 + m^3) - m\xi_d(\bar{\xi}_d^2 + m)}{\xi_d\bar{\xi}_d(\xi_d^2 - m)(\xi - m/\xi_d)} - \xi\frac{1 + m\xi^2}{\xi^2 - m}\frac{d\varphi_{im}}{d\xi}, \tag{11}$$

ξ_d is one of the two roots of the equation $z_d = R(\xi_d + m/\xi_d)$, such that $|\xi_d| \geqslant 1$, $z = a + r_0e^{i\theta}$ $z_d = a + re^{i\theta}$, and $A = Gbe^{i\theta}/[4\pi i(1-\nu)]$.

The force $F^{d-d}(r_k, r, \theta)$ that a dislocation located at the point (r_k,θ) exerts on the dislocation at the point (r,θ) can be represented as:

$$F^{d-d}(r_k, r, \theta) = b\sigma^{d}_{r\theta}(r_k, r, \theta), \tag{12}$$

where $\sigma^{d}_{r\theta}(r_k, r, \theta)$ is the stress that a dislocation located at the point (r_k,θ) creates in the point (r,θ) located in the

vicinity of the elliptical crack tip. The stress $\sigma^d_{r\theta}(r_k, r, \theta)$ follows [48] from:

$$\sigma^d_{r\theta} = \mathrm{Im}[(\bar{z}\varphi''_d(z) + \psi'_d(z))e^{2i\theta}], \tag{13}$$

where

$$\varphi_d(z) = A\ln(z - z_d) + \varphi_{im}(z),$$
$$\psi_d(z) = \bar{A}\ln(z - z_d) - A\frac{\bar{z}_d}{z - z_d} + \psi_{im}(z), \tag{14}$$

$z = a + re^{i\theta}$, $z_d = a + r_k e^{i\theta}$.

Formulae (5)–(14) allow one to calculate the total force F acting on the dislocation near the tip of an elliptical crack. For the examined case of an elongated crack, we also relate the applied load σ_0 to the generalized stress intensity factor K_I as follows [41]: $\sigma_0 = K_I/\sqrt{\pi a}$.

Let us assume that the emission of the $(N+1)$th dislocation ($N = 0, 1, 2, \ldots$) is possible if there is a region within the interval $r_d < r < d$, where this dislocation is repelled from the crack tip, that is:

$$F^{\mathrm{emit}}(r_{N+1}, \theta) + F^{im}(r_{N+1}, \theta) + \sum_{k=1}^{N} F^{d-d}(r_k, r_{N+1}, \theta) - (N+1)F^{d-d}(0, r_{N+1}, \theta) > 0. \tag{15}$$

In order to calculate the maximum number N_m of lattice dislocations that can be emitted along the same slip plane, we use the following calculation procedure. First, we specify the initial crack tip curvature ρ_0 prior to dislocation emission from the crack tip. We assume that the crack has already been blunted due to previous consecutive processes of dislocation emission and crack advance. Furthermore, we focus on the situation where dislocation emission occurs sufficiently fast, so that the applied tensile load (and its associated stress intensity factor K_I) does not change in the course of dislocation emission. Since the maximum value of K_I prior to dislocation emission is $K_{IC}(\rho)$, in this situation, K_I cannot exceed $K_{IC}(\rho)$. Therefore, in order to calculate the maximum number of dislocations that can be emitted from the crack tip, we put the stress intensity factor K_I to be equal to its maximum value $K_{IC}(\rho_0)$. In addition, as a first approximation, we assume that emission of every dislocation increases the crack tip curvature radius by $b\sin\theta$. In this case, the crack tip curvature radius after the emission of N dislocations is $\rho = \rho_0 + Nb\sin\theta$. Next, we verify validity of criterion (15) for the emission of the first dislocation. If this criterion is valid, we place the first dislocation at the distance d from the crack tip and verify validity of criterion (15) for the emission of the second dislocation. If this criterion is valid for the second dislocation, we calculate its equilibrium position and check the validity of criterion (15) for the emission of the third dislocation, and so on. The procedure is carried out for all the new emitted dislocations and ends when criterion (15) for the emission of a new dislocation stops being valid.

With this calculation procedure, we have calculated the maximum number N_m of lattice dislocations emitted along the same plane as a function of grain size d, for various initial crack tip curvature radii ρ_0, in nanocrystalline/UFG Al and α-Fe. We have used the following values of dislocation Burgers vector magnitude b:$b = 0.286$ nm for Al, and $b = 0.249$ nm for α-Fe. The dependences $N_m(d)$, for various ρ_0, are shown in Fig. 4a and b for the cases of Al and α-Fe, respectively. As can be seen, the maximum number N_m of lattice dislocations that can be emitted along the same plane increases with rising grain size d and/or initial curvature radius ρ_0 of the crack tip. The first effect has been demonstrated previously [28,35]. The second effect is associated with the fact that, when the crack tip curvature radius ρ increases, the critical stress intensity factor for crack growth in metals increases more rapidly than the critical stress intensity factor for dislocation emission [28]. As a result, in these materials, crack blunting, once started, promotes further dislocation emission and further crack blunting. This role of crack blunting is contrasted to the effect of grain size reduction in nanocrystalline solids, which hinders dislocation emission and promotes brittle fracture.

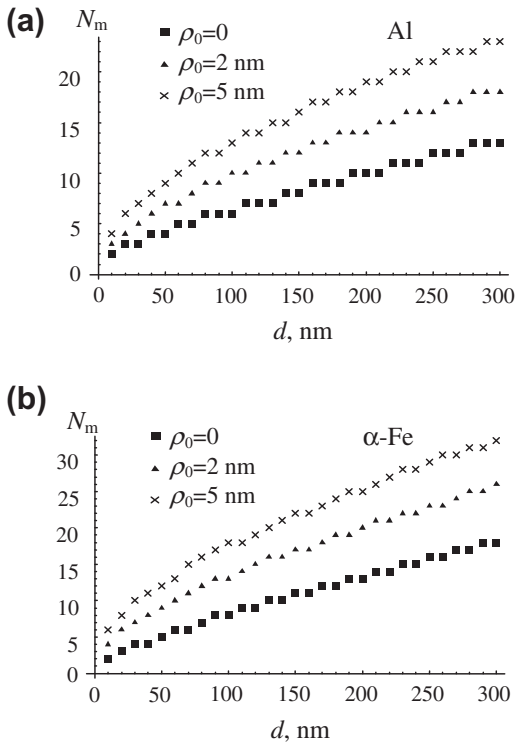

Fig. 4. Maximum number N_m of edge dislocations that can be emitted from the crack tip along one slip plane as functions of grain size d, for different crack tip curvature radii ρ_0, for: (a) Al and (b) α-Fe.

5. Effect of dislocation emission and crack blunting on critical stress intensity factor in nanocrystalline and ultrafine-grained materials

In the previous section, we have calculated the maximum number of dislocations that can be emitted from the tip of a blunt crack. In doing so, we assumed that, first, the crack has already been blunted due to previous consecutive processes of dislocation emission and crack advance,

and, second, that dislocation emission is so fast that the stress intensity factor K_I (associated with the applied load σ_0) does not change during the emission process. In this section, we consider another situation. We consider an initially sharp crack ($\rho_0 = 0$) which is then blunted due to the emission of dislocations from the crack tip along the same slip plane. In addition, we suppose that dislocation emission requires some time interval during which plastic deformation proceeds and the applied load can increase. As a consequence, the stress intensity factor K_I related to the applied load is also supposed to be able to increase during dislocation emission. In this case, the maximum number N_m of emitted dislocations corresponds to the situation where $K_I = K_{IC}(N)$, i.e. K_I reaches its critical value $K_{IC}(N)$ which grows with every new event of dislocation emission. We also calculate the increase in the critical stress intensity factor due to the dislocation emission along the same slip plane and associated crack blunting. It is clear that after the end of the dislocation emission process, the critical stress intensity factor is $K_{IC} = K_{IC}(N_m)$.

The calculation procedure for the situation examined in this section is identical to that described in the previous section, except for two aspects. First, here we change the value of K_I after the emission of each dislocation. Second, since the value of K_{IC} changes in the course of dislocation emission, K_{IC} is affected not only by the crack tip curvature radius ρ but also by the stress fields of the emitted dislocations.

In order to calculate K_{IC}, we consider the two cases: $\rho < \rho_c$ and $\rho > \rho_c$. Since $\rho = Nb \sin\theta$ in the examined case, the above two inequalities can be rewritten in terms of the number N of emitted dislocations as $N < \rho_c/(b \sin\theta)$ and $N > \rho_c/(b \sin\theta)$, respectively. By analogy with our examination in the previous section, the crack is viewed as sharp, if $\rho < \rho_c$, and crack blunting is taken into account, if $\rho > \rho_c$. In the case of the sharp crack ($\rho < \rho_c$), the critical stress intensity factor $K_{IC}(N)$ can be written as follows [50]:

$$K_{IC}(N) = \sqrt{(K_{IC}^{\mathrm{br}})^2 - \left(\sum_{i=1}^{N} k_{II}^d(r_i)\right)^2} - \sum_{i=1}^{N} k_I^d(r_i), \quad \rho < \rho_c, \tag{16}$$

where r_i is the coordinate of the ith dislocation, $K_{IC}^{\mathrm{br}} = \sqrt{4G\gamma/(1-\nu)}$, and $k_I^d(r_i)$ is the intensity factor of the tensile stress created by the ith dislocation near the crack tip. The stress intensity factors $k_I^d(r)$ and $k_{II}^d(r)$ appearing in formula (16) follow [51,52] as:

$$k_I^d(r) = -\frac{3\pi Db \sin\theta \cos(\theta/2)}{\sqrt{2\pi r}},$$
$$k_{II}^d = -\frac{\pi Db[\cos(\theta/2) + 3\cos(3\theta/2)]}{2\sqrt{2\pi r}}, \tag{17}$$

where $D = G/[2\pi(1 - \nu)]$.

In the case of the blunt crack ($\rho > \rho_c$), we will use the criterion $\sigma_{yy}(r = 0, \theta = 0) = \sigma_p$ of crack growth (see the previous section), where σ_{yy} is the total stress created by the applied load and the emitted dislocation. As a result, we can extend formula (2) to the case where dislocations are located near the crack tip as follows:

$$\sigma_{yy}(r = 0, \theta = 0) = \frac{2K_I}{\sqrt{\pi\rho}} + \sum_{i=1}^{N} \sigma_{yy}^d(r_i, 0, \theta) - (N+1) \lim_{r\to 0} \sigma_{yy}^d(0, r, \theta), \tag{18}$$

where $\sigma_{yy}^d(r_d, r, \theta)$ is the stress created in the point (r, θ) by a dislocation located at the point (r_d, θ). This stress is given [47] by:

$$\sigma_{yy}^d = \mathrm{Re}[2\varphi_d' + \bar{z}\varphi_d''(z) + \psi_d'(z)]. \tag{19}$$

With the relation $\sigma_{yy}(r = 0, \theta = 0)|_{K_I = K_{IC}} = \sigma_p$, formula (18) yields:

$$K_{IC}(N) = \sigma_p\sqrt{\pi\rho}/2 + \sum_{i=1}^{N} \sigma_{yy}^d(r_i, 0, \theta) - (N+1) \lim_{r\to 0} \sigma_{yy}^d(0, r, \theta), \quad \rho > \rho_c. \tag{20}$$

Formulae (16), (17), (19), and (20) give the critical stress intensity factor $K_{IC}(N)$ used in the numerical calculation of the equilibrium positions of subsequent emitted dislocations. The quantity $K_{IC}(N)$ also gives the critical stress intensity factor K_{IC} after the end of dislocation emission. It is defined as $K_{IC} = K_{IC}(N_m)$.

In the cases of Al and α-Fe, the critical stress intensity factors K_{IC} (which characterize the fracture toughness of nanocrystalline/UFG solids) are presented in Fig. 5 as functions of grain size d. As follows from Fig. 5, K_{IC} significantly increases with grain size d. In particular, an increase in grain size from 10 to 300 nm makes K_{IC} two or three times larger and thus dramatically enhances the toughness/ductility of the solid. Conversely, a decrease in grain size dramatically decreases K_{IC} and thus makes the solid much more brittle.

Fig. 5 demonstrates that, for UFG Al and α-Fe with a grain size of 300 nm, the calculated values of K_{IC} are around 1.2 and 4 MPa m$^{1/2}$, respectively. These values are still very small. In particular, they are more than an order of magnitude smaller than the experimental values of K_{IC} for conventional polycrystalline Al and α-Fe. At the same time, in calculating these values we have taken

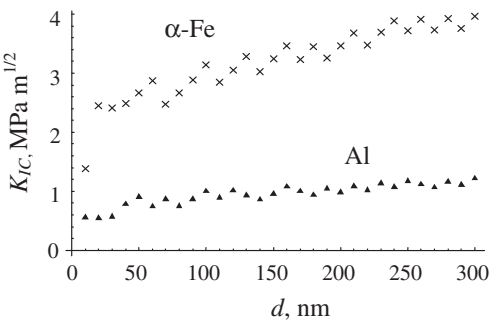

Fig. 5. Critical stress intensity factor K_{IC} vs. grain size in nanocrystalline/UFG Al and α-Fe.

into account dislocation emission only along one slip plane. Apparently, accounting for dislocation emission along multiple slip planes in the course of crack growth would increase the calculated values of K_{IC} and make the effect of grain size on fracture toughness (a decrease in K_{IC} with a decrease in grain size) even more pronounced. In particular, this is because emission along multiple slip planes, and thereby crack blunting, are enhanced with an increase in the size of a grain within which the crack grows. Moreover, intergranular fracturing and emission of lattice dislocations and twins from GBs significantly influence the behavior of nanocrystalline metals under a mechanical load, and the effects of these processes are especially pronounced when the grain size is in the interval $d < 30$ nm (e.g. [2,6,10,20,53–56]). For instance, the experimentally observed [20,57,58] generation of nanoscale cracks and voids at the triple junctions of GBs near the tips of growing blunt cracks releases the elastic energy near the tips of these cracks and thus hinders their growth. Emission of lattice dislocations and twins from GBs [55,56,59] causes a similar effect when the emission events occur near the tips of growing cracks in nanocrystalline materials. A detailed theoretical examination of the effects of dislocation emission along multiple slip planes, generation of triple junction voids and emission of lattice dislocations and twins from GBs on crack growth represents a very cumbersome problem, the analysis of which is beyond the scope of this paper. Here we focused on blunting of a crack through emission of lattice dislocations along one slip plane from the crack tip as the most typical process crucially influencing crack growth in nanocrystalline and UFG metals with grain sizes $d > 20$ nm at room temperature.

It should also be noted that the model used here implies that dislocations emitted from the crack tip are arrested at grain boundaries and do not interact with any pre-existing dislocations in grain interiors. This is the case if the grain size is sufficiently small, so that the dislocations in grains do not produce large pile-ups (which can penetrate from one grain to another one or initiate essential plastic deformation in the neighboring grains) and the dislocation density in grain interiors is small. At the same time, the suggested model is questionable for the solids with grain sizes that exceed several hundred nanometers.

6. Discussion and concluding remarks

We have theoretically revealed that the critical stress intensity factors K_{IC} (which characterize toughness) of nanocrystalline and UFG materials are highly sensitive to the grain size in these materials in a typical situation where crack blunting and growth processes are controlled by dislocation emission from crack tips. The sensitivity in question is caused by the grain-size-dependent effects of GBs and the crack blunting on the dislocation emission from crack tips. GBs effectively suppress both the dislocation emission from crack tips and thereby the blunting of cracks in nanocrystalline metals and ceramics with comparatively small grains. Furthermore, crack blunting (associated with the dislocation emission) hampers further dislocation emission from a crack tip and thereby further crack blunting. These combined effects of GBs and the crack blunting on further crack blunting are enhanced with decreasing the grain size (Fig. 5). As a corollary, when the grain size of a nanocrystalline/UFG solid decreases, cracks in this solid tend to be sharp, and the solid tends to show a brittle behavior. This theoretical conclusion is in good agreement with numerous experimental data confirming the discussed tendency [2,4–7,9,31,60–63]. In particular, the conclusion is supported by the experimentally detected fact [11–13] that some nanocrystalline fcc metals exhibit a ductile-to-brittle transition with decreasing grain size.

It should be noted that there are several examples of nanomaterials showing both superior strength and good ductility at room temperature or even superplasticity at elevated temperatures [20,30,33,64–79]. In these examples, good ductility/superplasticity is exhibited by UFG ceramics [62–66] and metallic materials [30,33,76,78,79] (with the mean grain size ranging from 100 nm to 1 μm) as well as by nanocrystalline ceramics [71,72,75] and metallic materials [1,20,67–70,73,74,77] (with the mean grain size ranging from 5 to 100 nm). Based on the results of the theoretical analysis given in this paper, crack blunting through lattice dislocation emission from crack tips contributes to enhanced ductility of UFG materials. At the same time, good ductility/superplasticity of nanocrystalline materials, especially those with the finest grains (grain size below 20 nm), is hardly related to crack blunting through lattice dislocation slip. In nanocrystalline materials with the finest grains, in parallel with lattice dislocation slip, such plastic flow micromechanisms as GB sliding, GB diffusional creep, stress-driven GB migration, twin and rotation deformation modes effectively operate [2,4–7,9,31,60–63]. These micromechanisms can be responsible for ductile behavior and high fracture toughness of such materials under certain conditions. In particular, in recent years, stress-driven GB migration [80], GB sliding [81–83] and twin deformation [59] have been recognized as plastic flow micromechanisms capable of enhancing fracture toughness in nanocrystalline metals and ceramics [59,80]. In addition, twin deformation [76,78] and GB sliding [84,85] can cause strain hardening, which suppresses plastic strain instability and the corresponding neck formation responsible for the low ductility of nanocrystalline materials under tensile deformation.

Furthermore, our theoretical results on the sensitivity of fracture toughness to grain size are relevant in interpretation of experimentally observed [61,68,86–88] ductile behavior exhibited by nanomaterials with a bimodal structure consisting of micron-sized grains embedded into a nanocrystalline matrix. In short, our results confirm the natural suggestion (formulated in the pioneering papers on nanomaterials with a bimodal structure [86,88]) that cracks in such materials are effectively stopped within large grains, in which case nanomaterials with a bimodal structure have good toughness.

To summarize, in a typical situation where crack blunting and growth processes are controlled by dislocation emission from crack tips, grain size reduction causes nanocrystalline materials to show a brittle behavior. At the same time, in the opposite situation where crack blunting and growth processes are strongly influenced or even controlled by alternate deformation modes (e.g. stress-driven GB migration, GB sliding, twin deformation), these deformation modes are capable of causing good ductility/toughness of nanocrystalline and UFG materials under certain conditions. The theory of the toughness of nanocrystalline and UFG materials deformed by alternative deformation modes is in its infancy [59,80–83] and needs further development in the future.

Acknowledgements

The work was supported, in part, by the Russian Foundation of Basic Research (Grant 08-01-00225-a), the National Science Foundation (Grant CMMI #0700272), the Russian Federal Agency of Science and Innovations (Grant MK-1702.2008.1), and the Russian Academy of Sciences Program "Fundamental Studies in Nanotechnologies and Nanomaterials".

References

[1] Mukherjee AK. Mater Sci Eng A 2002;322:1.
[2] Kumar KS, Suresh S, Van Swygenhoven H. Acta Mater 2003;51:5743.
[3] Kuntz JD, Zhan G-D, Mukherjee AK. MRS Bull 2004;29:22.
[4] Ovid'ko IA. Int Mater Rev 2005;50:65.
[5] Wolf D, Yamakov V, Phillpot SR, Mukherjee AK, Gleiter H. Acta Mater 2005;53:1.
[6] Meyers MA, Mishra A, Benson DJ. Prog Mater Sci 2006;51:427.
[7] Dao M, Lu L, Asaro RJ, De Hosson JTM, Ma E. Acta Mater 2007;55:4041.
[8] Koch CC. J Mater Sci 2007;42:1403.
[9] Koch CC, Ovid'ko IA, Seal S, Veprek S. Structural nanocrystalline materials: fundamentals and applications. Cambridge: Cambridge University Press; 2007.
[10] Ovid'ko IA. J Mater Sci 2007;42:1694.
[11] Li H, Ebrahimi F. Appl Phys Lett 2004;84:4307.
[12] Li H, Ebrahimi F. Adv Mater 2005;17:1969.
[13] Ebrahimi F, Liscano AJ, Kong D, Zhai Q, Li H. Rev Adv Mater Sci 2006;13:33.
[14] Rice JR, Thompson RM. Philos Mag 1974;29:73.
[15] Horton JA, Ohr SM. J Mater Sci 1982;17:3140.
[16] Rice JR. J Mech Phys Sol 1992;40:239.
[17] Armstrong RW. Metall Mater Trans A 1970;1:1169.
[18] Armstrong RW. In: Baker TN, editor. Yield, flow and fracture of polycrystals. Barking: Applied Science; 1983. p. 1–31.
[19] Weissmüller J, Markmann J. Adv Eng Mater 2005;7:202.
[20] Kumar KS, Suresh S, Chisholm MF, Horton JA, Wang P. Acta Mater 2003;51:387.
[21] Li WL, Li JCM. Philos Mag A 1989;59:12451261.
[22] Noronha SJ, Farkas D. Phys Rev B 2002;66:132103.
[23] Zeng XH, Hartmaier A. Acta Mater 2010;58:301.
[24] Ritchie RO, Horn RM. Metall Trans A 1978;9:331.
[25] Pandey RK. J Mater Sci 1984;19:607.
[26] Swanson RE, Thompson AW, Bernstein IM. Metall Trans A 1986;17:1633.
[27] Yoda M. Eng Fract Mech 1987;26:425.
[28] Ovid'ko IA, Sheinerman AG. Scripta Mater 2009;60:627.
[29] Valiev RZ, Islamgaliev RK, Alexandrov IV. Prog Mater Sci 2000;45:103.
[30] Valiev RZ. Nature Mater 2004;3:511.
[31] Figueiredo RB, Kawasaki M, Langdon TG. Rev Adv Mater Sci 2009;19:1.
[32] Horita Z, Furukawa M, Nemoto M, Barnes AJ, Langdon TG. Acta Mater 2000;48:3633.
[33] Valiev RZ, Alexandrov IV, Zhu YT, Lowe TC. J Mater Res 2002;17:5.
[34] Kawasaki M, Langdon TG. J Mater Sci 2007;42:1782.
[35] Beltz GE, Lipkin DM, Fischer LL. Phys Rev Lett 1999;82:4468.
[36] Latapie A, Farkas D. Phys Rev B 2004;69:134110.
[37] Huang M, Li Z. J Mech Phys Solids 2004;52:1991.
[38] Creager M, Paris PC. Int J Fract 1967;3:247.
[39] Armstrong RW. Eng Fract Mech 1987;28:529.
[40] Anderson TL. Fracture mechanics: fundamentals and applications. Boca Raton, FL: Taylor & Francis; 2005.
[41] Panasyuk VV, editor. Fracture mechanics and strength of materials. Kiev: Naukova Dumka; 1974 [in Russian].
[42] Eshelby JD. In: Nabarro FRN, editor. Dislocations in solids, vol. 1. Amsterdam: North-Holland; 1980. p. 167–222.
[43] Frank FC. Acta Cryst 1951;4:497.
[44] Huang XR, Dudley M, Vetter WM, Huang W, Wang S, Carter CH. Appl Phys Lett 1999;74:353.
[45] Gutkin MY, Sheinerman AG, Argunova TS, Mokhov EN, Je JH, Hwu Y, et al. J Appl Phys 2003;94:7076.
[46] Ma X. J Appl Phys 2006;99:063513.
[47] Muskhelishvili NI. Some basic problems on the mathematical theory of elasticity: fundamental equations, plane theory of elasticity, torsion and bending. Holland: Noordhoff; 1975.
[48] Fisher LL, Beltz GE. J Mech Phys Sol 2001;49:635.
[49] Hirth JP, Lothe J. Theory of dislocations. New York: Wiley; 1982.
[50] Morozov NF, Ovid'ko IA, Sheinerman AG, Aifantis EC. Mater Phys Mech 2009;8:155.
[51] Lin I-H, Thomson R. Acta Metall 1986;34:187.
[52] Zhang T-Y, Li JCM. Acta Metall Mater 1991;39:2739.
[53] Ovid'ko IA, Sheinerman AG. Acta Mater 2004;52:1201.
[54] Ovid'ko IA, Sheinerman AG. Acta Mater 2005;53:1359.
[55] Asaro RJ, Suresh S. Acta Mater 2005;53:3369.
[56] Zhu B, Asaro RJ, Krysl P, Bailey P. Acta Mater 2005;53:4825.
[57] Milligan WW, Hackney SA, Ke M, Aifantis EC. Nanostruct Mater 1993;2:267.
[58] Ke M, Milligan WW, Hackney SA, Carsley JE, Aifantis EC. Nanostruct Mater 1995;5:689.
[59] Gutkin MY, Ovid'ko IA, Skiba NV. Philos Mag 2008;88:1137.
[60] Zhan G-D, Kuntz JD, Mukherjee AK. MRS Bull 2004;29:22.
[61] Han BQ, Lavernia E, Mohamed FA. Rev Adv Mater Sci 2005;9:1.
[62] Ovid'ko IA. Rev Adv Mater Sci 2005;10:89.
[63] Weng GJ. Rev Adv Mater Sci 2009;19:41.
[64] Wakai F, Sakagachi S, Matsuno Y. Adv Ceram Mater 1986;1:259.
[65] Wakai F, Kato H. Adv Ceram Mater 1988;3:71.
[66] Kondo N, Wakai F, Nishioka T, Yamakawa A. J Mater Sci Lett 1995;14:1369.
[67] Karimpoor AA, Erb U, Aust KT, Palumbo G. Scripta Mater 2003;49:651.
[68] Wang YM, Ma E. Acta Mater 2004;52:1699.
[69] Youssef K-M, Scattergood RO, Murty KL, Koch CC. Appl Phys Lett 2004;85:929;
Youssef K-M, Scattergood RO, Murty KL, Koch CC. Scripta Mater 2006;54:251.
[70] Youssef KM, Scattergood RO, Murty KL, Horton JA, Koch CC. Appl Phys Lett 2005;87:091904.
[71] Zhan GD, Garay JE, Mukherjee AK. Nano Lett 2005;5:2593.
[72] Zhou X, Hulbert DM, Kuntz JD, Sadangi RK, Shukla V, Kear BH, et al. Mater Sci Eng A 2005;394:353.
[73] Sergueeva AV, Mukherjee AK. Rev Adv Mater Sci 2006;13:1.
[74] Sergueeva AV, Mara NA, Krasilnikov NA, Valiev RZ, Mukherjee AK. Philos Mag 2006;86:5797.

[75] Xu X, Nishimura T, Hirosaki N, Xie RJ, Yamamoto Y, Tanaka H. Acta Mater 2006;54:255.
[76] Zhao YH, Bingert JF, Liao XZ, Cui K, Han AV, Sergueeva, et al. Adv Mater 2006;18:2949.
[77] Zhao YH, Liao XZ, Cheng S, Ma E, Zhu YT. Adv Mater 2006;18:2280.
[78] Zhao YH, Zhu YT, Liao XZ, Horita Z, Langdon TG. Appl Phys Lett 2006;89:121906.
[79] Zhao YH, Bingert JF, Zhu YT, Liao XZ, Valiev RZ, Horita Z, et al. Appl Phys Lett 2008;92:081903.
[80] Ovid'ko IA, Sheinerman AG, Aifantis EC. Acta Mater 2008;56:2718.
[81] Yang F, Yang W. Int J Solids Struct 2008;45:3897.
[82] Yang F, Yang W. J Mech Phys Solids 2009;57:305.
[83] Bobylev SV, Mukherjee AK, Ovid'ko IA, Sheinerman AG. Rev Adv Mater Sci 2009;21:99.
[84] Ovid'ko IA, Sheinerman AG. Appl Phys Lett 2007;90:171927.
[85] Ovid'ko IA, Sheinerman AG. Acta Mater 2009;57:2217.
[86] Tellkamp VL, Melmed A, Lavernia EJ. Metall Mater Trans A 2001;32:2335.
[87] Wang Y, Chen M, Zhou F, Ma E. Nature 2002;419:912.
[88] Han BQ, Lee Z, Witkin D, Nutt SR, Lavernia EJ. Metall Mater Trans A 2005;36:957.